Electric field dependence of optical absorption near the band gap of quantum-well structures

D. A. B. Miller, D. S. Chemla, and T. C. Damen
AT&T Bell Laboratories, Holmdel, New Jersey 07733

A. C. Gossard and W. Wiegmann
AT&T Bell Laboratories, Murray Hill, New Jersey 07974

T. H. Wood and C. A. Burrus
AT&T Bell Laboratories, Crawford Hill, New Jersey 07733
(Received 4 March 1985)

We report experiments and theory on the effects of electric fields on the optical absorption near the band edge in GaAs/AlGaAs quantum-well structures. We find distinct physical effects for fields parallel and perpendicular to the quantum-well layers. In both cases, we observe large changes in the absorption near the exciton peaks. In the parallel-field case, the excitons broaden with field, disappearing at fields $\sim 10^4$ V/cm; this behavior is in qualitative agreement with previous theory and in order-of-magnitude agreement with direct theoretical calculations of field ionization rates reported in this paper. This behavior is also qualitatively similar to that seen with three-dimensional semiconductors. For the perpendicular-field case, we see shifts of the exciton peaks to lower energies by up to 2.5 times the zero-field binding energy with the excitons remaining resolved at up to $\sim 10^5$ V/cm: This behavior is qualitatively different from that of bulk semiconductors and is explained through a mechanism previously briefly described by us [D. A. B. Miller *et al.*, Phys. Rev. Lett. 53, 2173 (1984)] called the quantum-confined Stark effect. In this mechanism the quantum confinement of carriers inhibits the exciton field ionization. To support this mechanism we present detailed calculations of the shift of exciton peaks including (i) exact solutions for single particles in infinite wells, (ii) tunneling resonance calculations for finite wells, and (iii) variational calculations of exciton binding energy in a field. We also calculate the tunneling lifetimes of particles in the wells to check the inhibition of field ionization. The calculations are performed using both the 85:15 split of band-gap discontinuity between conduction and valence bands and the recently proposed 57:43 split. Although the detailed calculations differ in the two cases, the overall shift of the exciton peaks is not very sensitive to split ratio. We find excellent agreement with experiment with no fitted parameters.

I. INTRODUCTION

The electric-field dependence of optical absorption (electroabsorption) near the optical band edge in semiconductors is a subject which has been extensively studied both theoretically and experimentally. In bulk semiconductors, the resultant shift and broadening of the band edge absorption is usually known as the Franz-Keldysh effect.[1,2] In relatively pure semiconductors especially at low temperature, the absorption edge in direct-gap semiconductors can be dominated by the exciton absorption resonances corresponding to the creation of an electron and hole in a hydrogenic orbit. To model the electroabsorption properly, these excitonic effects must be included (see, for example, Dow and Redfield[3]). At relatively low fields, the electroabsorption can actually be dominated by excitonic resonance effects; the $1S$ peak initially shifts to lower energy and broadens.[3,4] This behavior can be explained as a Stark shift of the $1S$ hydrogenic exciton level coupled with a broadening. The analogy between Stark shifts in real atomic systems and the shifts seen in excitons is formally exact within the effective-mass approximation. One practical difference is that, with the exciton, we measure the true shift of the $1S$ ground state, not the difference in the shifts of two atomic states as is common in atomic spectroscopy. The $1S$ peak can shift by only $\sim 10\%$ of the exciton binding energy before the broadening becomes so severe that the peak becomes unresolvable at a few times the classical ionization field. This (Stark) broadening (see, for example, Vrehen[4]) is essentially due to the reduction of lifetime of the exciton resulting from field ionization by the applied electric field; with a uniform applied field there are no longer truly any bound states of the electron-hole system as the particles can tunnel through the resulting distorted Coulomb potential barrier.[3]

In recent years, semiconductor growth technology has advanced to such an extent that it is now possible to grow thin-layered semiconductor structures of very high quality. These layers can be controllably so thin that particle-in-a-box confinement of electrons and holes can readily be seen (see, for example, Dingle *et al.*[5]). With the GaAs/AlGaAs material system, because the larger band-gap AlGaAs "barriers" have both lower valence-band edges and higher conduction-band edges than the GaAs, the alternate thin layers result in confinement of both

electrons and holes within the GaAs layers (or "wells"). Consequently, excitons may also be confined within the GaAs layers. If the AlGaAs barriers are sufficiently thick, and have a sufficiently large Al concentration so that the potential barriers are high, then penetration of the wave functions from one GaAs layer (or quantum well) to another may be neglected at least for the low-energy states within the quantum well; then we may refer to the structure as a multiple quantum-well structure (MQWS). The physics of such a MQWS for these low-energy states is for many purposes the physics of a single quantum well although it is convenient for optical-absorption studies to grow a MQWS to obtain sufficient optical absorption. (If the wave-function penetration is significant, then superlattice effects become important and the physics is qualitatively different.)

The MQWS growth can be of such high quality that exciton resonances can be clearly seen even for layer thicknesses much less than the usual three-dimensional (3D) exciton diameter (~ 300 Å in bulk GaAs). The question therefore arises as to what will be the electroabsorptive effects in such MQWS's. Clearly because of the quantum confinement the physics may be qualitatively different. It is also immediately obvious that there are two distinct physical configurations in the MQWS compared to the bulk, namely (i) electric field parallel to the quantum-well layers and (ii) electric field perpendicular to the layers, and we may expect different physical effects in each case.

One remarkable phenomenon which makes the MQWS electroabsorption of further interest is that in both GaAs/AlGaAs MQWS's[6–8] and very recently in InGaAs/InAlAs MQWS's[9] the exciton resonances can be clearly observed at room temperature. This is remarkable because in GaAs (and most other bulk semiconductors) the exciton resonance is all but unresolvable at room temperature and in InGaAs it is barely resolvable even at low temperature. The physical reasons for this are interesting in themselves (see, for example, Refs. 6 and 10) but the observation is of potential practical importance as it may enable the development of room-temperature optical devices utilizing excitons. Indeed, some nonlinear optical devices have already been demonstrated[10–15] and, more importantly for the present discussion, several speculative optical modulators[16–18] and switches[19] have already been demonstrated utilizing electroabsorptive effects in GaAs/AlGaAs MQWS's.

The aim of this paper is therefore to investigate both experimentally and theoretically the parallel- and perpendicular-field electroabsorptive effects in MQWS's. We will use GaAs/AlGaAs MQWS's throughout (at room temperature) although the theoretical models are of more general applicability. We will find that the parallel-field case is qualitatively similar to the electroabsorption in bulk materials, but the perpendicular-field case is significantly different, and appears to be best described as a separate mechanism, at least for wells that are thin compared to the 3D exciton diameter. This new mechanism we call the quantum-confined Stark effect (QCSE). We have briefly discussed this mechanism[20] before. It can explain the remarkable persistence of the exciton resonances to very high fields (~ 50 times the classical ionization field, E_i) with correspondingly large energy shifts (up to 2.5 times the zero-field exciton binding energy), which empirically distinguishes this electroabsorption from the bulk electroabsorptive effects described above. The general theoretical formalism we use is all within the effective-mass approximation, so the theoretical discussion will reduce largely to a treatment of a hydrogenic system with quantum confinement and an applied electric field (hence, the title QCSE for the perpendicular-field electroabsorption). In principle, much of the theory extends therefore to the hydrogen atom, and the large size and small binding energy of the exciton enables us to test the theory at relative fields (e.g., $50E_i$) and quantum confinements (e.g., confinement within $\frac{1}{3}$ of the 3D hydrogenic diameter) which are currently unattainable for an actual hydrogen atom.

The effect of electric fields on the optical properties of MQWS's has previously been considered by several authors both experimentally[16,20–25] and theoretically.[16,20,25–28] Prior to our own first observations of electric-field dependence of optical absorption in MQWS's,[16] measurements were made of the changes in luminescence with electric field at low temperature.[21,22] Insight was gained into impurities using this technique[22] and quenching of luminescence was observed at very moderate electric fields.[21,22] Partly in an attempt to explain the luminescence quenching, variational calculations were made[26] of the changes in wave functions and energies of the particle-in-a-box envelope functions with applied field. The quenching of the luminescence, which may in fact be due to the sweeping out of carriers by the applied field,[26] unfortunately limits this technique to low fields, and luminescence techniques at room temperature are often more difficult anyway. The variational theory[26] itself is of more general use, and we will use and extend some of its results as part of the theory in this work. Independently of our own work,[20] this theory was also recently[27] extended to attempt to fit our early electroabsorption data.[16] Absorption measurements[16,20] have the advantage that they can conveniently be made at room temperature and also we find in practice that they give useful information up to much higher fields than the first luminescence studies.[21,22] Other luminescence studies have also been performed[24,28] under conditions designed to prevent the sweeping out of carriers encountered in the previous luminescence work.[26]

The reasons why we should expect to see interesting physical phenomena with moderate electric fields become clear from simple order-of-magnitude arguments. For typical quantum-well widths (e.g., ≈ 100 Å) in GaAs/AlGaAs MQWS's, both the exciton and the individual electrons and holes have envelope functions and energy levels of comparable magnitudes. Exciton binding energies are ≈ 10 meV; the confinement energies of the first subbands are ≈ 5—50 meV for electrons and holes. The radial exciton envelope wave functions are ≈ 100 Å diameter and the envelope functions of the carriers in the wells have an extent perpendicular to the layers comparable to the well width (e.g., ≈ 100 Å). Consequently, applying fields ≈ 10 meV/100 Å (i.e., 1 V/μm or 10^4 V/cm)

should produce large perturbations of these wave functions.

The structure of this paper is as follows. In Sec. II, we discuss the samples and other experimental details. In Sec. III the experimental results are presented. In Sec. IV, we discuss the theory of the various effects and compare this with the experimental results. Section V presents the conclusions of the work. Several theoretical models were developed to explain the results, and the detailed derivations and general results of these models are discussed in the four Appendixes. Appendix A treats the field ionization of a two-dimensional exciton in a parallel field. Appendix B derives the exact theory of the perpendicular-field dependence of confined states in a well of infinite depth. Exact calculations by a tunneling resonance method of the shifts and widths of energy levels in realistic finite wells (with perpendicular field) are presented in Appendix C for an effective-mass model. Finally in Appendix D the change in exciton binding energy (for perpendicular fields), due to the separation of electron and hole, is calculated variationally.

II. EXPERIMENTAL DETAILS

A. Samples

Two samples were grown by molecular-beam epitaxy on (100) GaAs substrates, one for each field configuration. In both cases, the active MQWS material consists of alternate thin layers of GaAs wells and $Al_xGa_{1-x}As$ barriers with sufficient GaAs layers to give about one optical-absorption length of optical thickness in the spectral range of interest near to the optical-absorption edge. In order to be able to see through the sample in this region, it is necessary to remove the GaAs substrate over at least some fraction of the sample area. Hence, a layer consisting either totally or predominantly of AlGaAs is grown in each case next to the GaAs substrate to serve as an etch stop layer when using a selective GaAs etchant. This layer itself is transparent at the wavelengths of interest. In both cases, the samples have been designed to minimize electrical heating which could otherwise complicate interpretation of the spectra. They were grown with substrate temperatures of 700 °C under arsenic-rich growth conditions employing an As_2 beam.

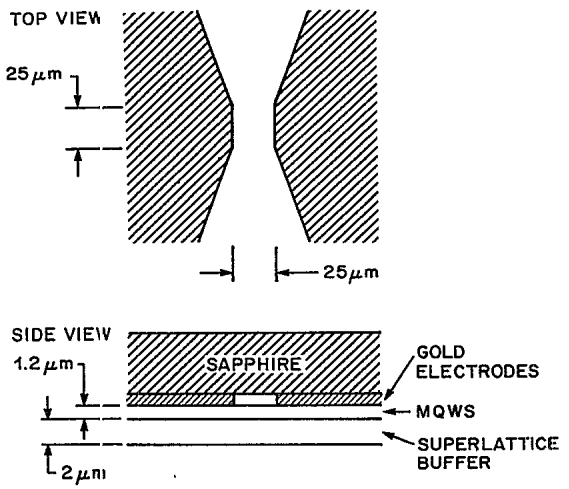

FIG. 1. Schematic of the sample used for parallel-field experiments (not to scale). The 2-μm superlattice (SL) buffer consisted of layers, 14 Å thick, of GaAs separated by 182-Å $Al_{0.32}Ga_{0.68}As$ layers. The MQW region consisted of 60 layers, 95 Å thick, of GaAs separated by 98-Å $Al_{0.32}Ga_{0.68}As$ layers.

The material for the parallel-field sample consists of a superlattice etch stop layer and a set of active quantum wells grown on a semi-insulating, Cr-doped GaAs substrate. The superlattice material is primarily AlGaAs but contains very thin layers of GaAs. The use of superlattice material rather than simple AlGaAs may help to reduce the background concentration of impurities and also improve the quality of the first few quantum wells. The exact parameters of the material itself are given in Fig. 1. This material has no intentional doping.

To apply electric fields parallel to the quantum-well layers, we applied electrodes to a $\approx 3 \times 6$ mm piece of material as shown in Fig. 1. Zinc-doped gold electrodes were evaporated and alloyed into the material. More gold was electroplated and evaporated around the sides and onto the back of the material so that the sample could be electrically contacted after being glued down. Then, the material was epoxied to a sapphire substrate and a ≈ 2 mm wide strip of the GaAs substrate above the electrode gap was removed by the selective etch[29] to leave good optical access to the $\approx 25 \times 25$ μm electrode gap. The resulting sample was electrically ohmic at low voltages with a resistance ≈ 15 MΩ. Since the sample is Ohmic this suggests that the background doping in the MQWS is p type because the zinc-doped gold should give p-type contact regions. This sample overcomes several problems encountered with previous samples.[23] The high resistance of the sample combined with the relatively high thermal conductivity of the sapphire substrate reduces any thermal effects. The alloyed contacts eliminate Schottky barriers which can confuse the estimation of field magnitude and direction.

To apply fields perpendicular to the quantum-well layers we initially simply applied semitransparent electrodes above and below MQWS material. However, even with high resistivity material, we found that such a structure has low resistance unless the area of the device is made very small. We were able to resolve some effects on optical absorption which we believe were due to electric fields, but the Ohmic heating was large and interpretation of the results was unreliable. Consequently we designed material in which the MQWS was contained primarily within the depletion region of a p-i-n diode so that substantial fields could be applied by reverse biasing the diode without significant conduction and electrical heating.

The final material parameters for the perpendicular-field sample are given in Fig. 2. p- and n-doped AlGaAs layers form the outer parts of the p and n regions of the diode, with the n-AlGaAs layer also acting as the etch stop layer. Initially we were concerned that the field in the depletion region might be so large as to destroy the absorption features of interest, so we inserted buffer layers which could enable us to move the highest field part of the depletion region outside the MQWS material. To allow for the background doping being either lightly n or

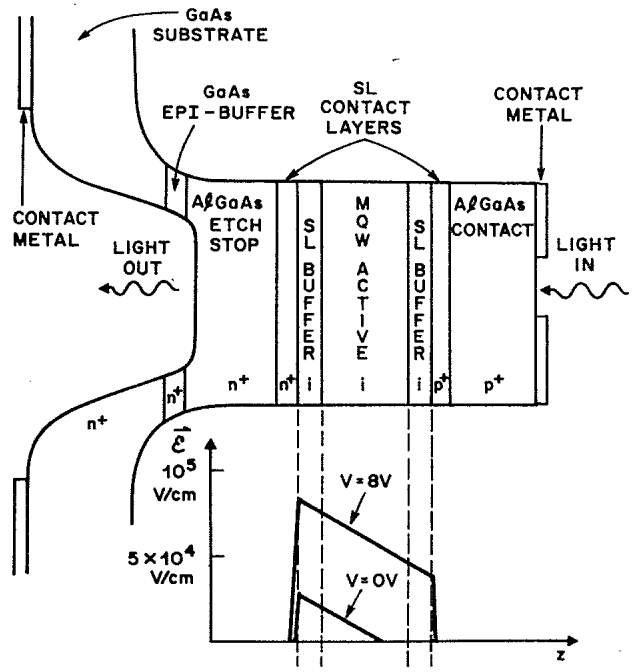

FIG. 2. Schematic of the sample used for perpendicular-field experiments (not to scale). The lower portion of the figure shows the calculated electric-field strength, E, as a function of position within the device for two applied voltages, using the depletion approximation. Sample parameters are MQWS active region: thickness 0.97 μm (50 periods 95 Å GaAs and 98 Å AlGaAs). Mole fraction of Al in AlGaAs is 0.32. Total thickness 3.9 μm. AlGaAs etch stop and top contact layers each 0.98 μm thick. Super lattice consists of 29-Å GaAs layers alternating with 69-Å AlGaAs layers. SL buffers: thickness (each) 0.29 μm (30 periods). SL contacts: thickness (each) 9.2 μm (20 periods). Substrate: Si-doped mesa diameter: 600 μm. Top contact opening diameter: 175 μm.

lightly p in the MQWS, we grew buffers on both sides of the MQWS. Again to reduce background impurity concentrations and improve the quality of the first few wells, we used superlattice material for the buffers and also carried this material on into the contact regions. The structure of the final perpendicular-field sample is shown in Fig. 2. A 600-μm-diameter mesa was etched down through the p-i-n diode material and this was contacted with a gold electrode with a $\approx$100-μm-diameter hole in the center to allow optical access. Then, a hole was etched in the substrate from behind using the selective etch to give optical access from this side. All the contact and buffer regions are transparent at the wavelengths of interest. The other contact on this structure was taken off the substrate which was n doped.

One disadvantage of the p-i-n configuration is that the electric field is not totally uniform within the i region due to finite background doping. Using C-V measurements, we deduced a background impurity concentration $\approx 2\times10^{15}$ cm^{-3} in the i region and the resulting calculated field distribution for two voltages is shown in Fig. 2. All fields quoted below for this sample are simple (linear) average fields in the MQWS. This structure behaved well as a diode with $\approx$100-nA reverse leakage and $\approx$40-V reverse breakdown, although it was far from the ideal diode law behavior in forward bias. This sample is similar to that used by us in modulator experiments.[16]

B. Measurement techniques

All the optical measurements were made using a continuous-wave infrared dye laser, pumped by a krypton ion laser and using LDS 821 dye, as the light source. This could be scanned over the wavelength region of interest. The use of a laser makes it easy to focus to the necessary small spot sizes, and the tunability of the source is particularly important for photocurrent spectra. Optical detection was by silicon photodiodes; for high-speed and/or high-sensitivity measurements an avalanche photodiode was used. Absolute powers were measured using a UDT 161 power meter with a calibrated silicon detector. Photocurrents were measured directly using a Keithley 195 digital multimeter. Differential absorption spectra were measured by using a square wave oscillator as the voltage source driving the samples and synchronously detecting the change in transmission of the samples with a lock-in amplifier; a portion of the input beam was split off, mechanically chopped, and detected on a reference detector using another lock-in amplifier to give a reference signal both for the differential spectra and photocurrent spectra. Absolute absorption spectra were measured using a dual-channel boxcar with one channel for the transmitted signal and the other for the reference. For spectra taken with a dc bias voltage, the optical beams were mechanically chopped and the boxcar was synchronized to the chopper. For spectra taken with a pulsed bias, the boxcar was synchronized to the pulse generator. All the spectra with perpendicular fields were measured with a dc bias. The spectra given here for the parallel field were taken with a pulsed bias to minimize heating effects and reduce the risk of damage to the sample given the high voltages sometimes used for these spectra. Spectra were also measured with dc bias at the lower bias for the parallel field sample to check the consistency of the results. All the spectra were taken with series resistors to protect the samples. The voltage drop across the resistor was kept below 1 V for the parallel field and below 0.1 V for the perpendicular field.

III. EXPERIMENTAL RESULTS

A. Parallel field

The principal results of the experiment for electric fields parallel to the quantum-well layers are summarized in the set of absorption spectra in Fig. 3. With increasing applied electric field, the absorption spectrum changes progressively from the low-field situation where the light- and heavy-hole exciton peaks are clearly resolved to the high-field situation where the exciton resonances are clearly destroyed and absorption has increased below and above the former position of the exciton resonances. By inspection of the spectra in Fig. 3 it is apparent that the dominant effect is a broadening of the absorption features with applied field. Large changes in the form of the spectrum are clearly seen with $\approx 1.6\times10^4$ V/cm (40 V). This

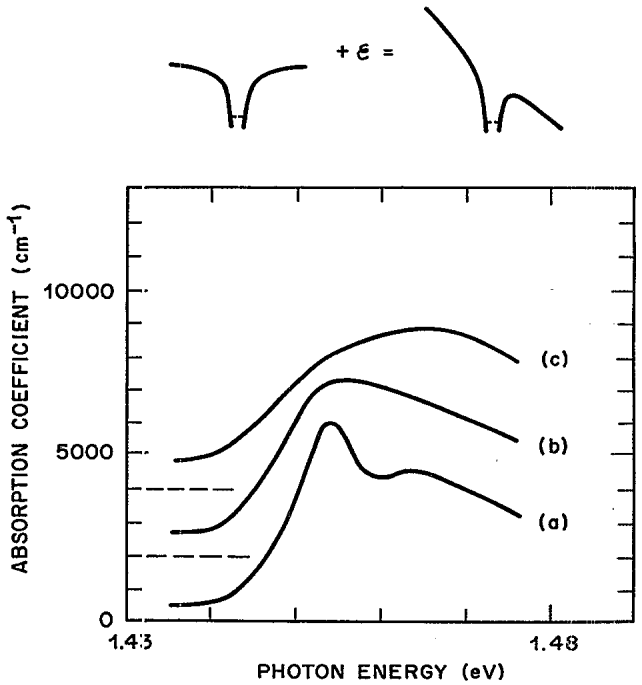

FIG. 3. Absorption spectra at various electric fields for the parallel-field sample. (a) 0 V/cm; (b) 1.6×10^4 V/cm; (c) 4.8×10^4 V/cm. The insert shows schematically the distortion of the Coulomb potential of electron and hole with applied field. The zeros are displaced for clarity as shown by the dashed lines.

can be seen more clearly in the differential spectrum shown in Fig. 4 which is taken with ≈ 8 kV/cm. We will discuss the detailed fitting of this differential spectrum in Sec. IV, but it is clear by inspection that broadening is playing a major role; we see increases in transmission at the exciton peak positions and decreases both above and below each peak as expected for broadening.

The spectra in Fig. 3 were taken with pulsed bias in 50-μs pulses spaced 700 μs apart with the optical transmission sampled by the boxcar ≈ 15 μs after the start of the pulse. Under these electrical conditions, the sample was Ohmic up to ≈ 60 V; above this voltage the current started to rise steeply reaching ≈ 10 μA with 80 V applied and above 100 V the current showed clear instabilities developing during the bias pulse. With dc bias, significant nonlinear increase in the current was seen above ≈ 30 V. Although the details of this electrical behavior are not yet understood, we believe that electrical heating is not responsible for the observed changes in spectra for several reasons. First, we know from independent experiments that heating produces primarily a shift of the spectrum in contrast to the observed broadening. Second, we find the same effects within experimental error for dc and pulsed bias, although we restricted the dc measurements to $\lesssim 20$-V bias to avoid any possibility of damaging the sample. Third, we have tested the optical response of the sample down to a pulse-generator-limited risetime of ≈ 10 ns with no measurable change in the degree of modulation of the transmitted light; even with 80-V bias where we measure currents of ≈ 10 μA, the total dissipated energy in 10 ns (≈ 8 pJ) would only be sufficient to raise the temperature of the volume of material in the 25-μm square between the electrodes by ≈ 20 mK even neglecting any further heat conduction, this is insufficient to make any large change in the spectra. The optical power is negligibly small in the measurements (400 nW) and we saw no significant changes in behavior as the spot size was altered from ≈ 3 μm diameter up to ≈ 20 μm diameter or as the spot was moved within the ≈ 25 μm square between the electrodes except for some overall changes which we ascribed to Fabry-Perot effects (the sample has no antireflection coatings).

The spectra of Figs. 3 and 4 were taken with the static electric field and the optical electric-field polarization perpendicular. However, we were not able to resolve any significant differences in electric-field dependence of absorption with the other optical-field polarization despite the fact that the symmetry is broken by the applied field.

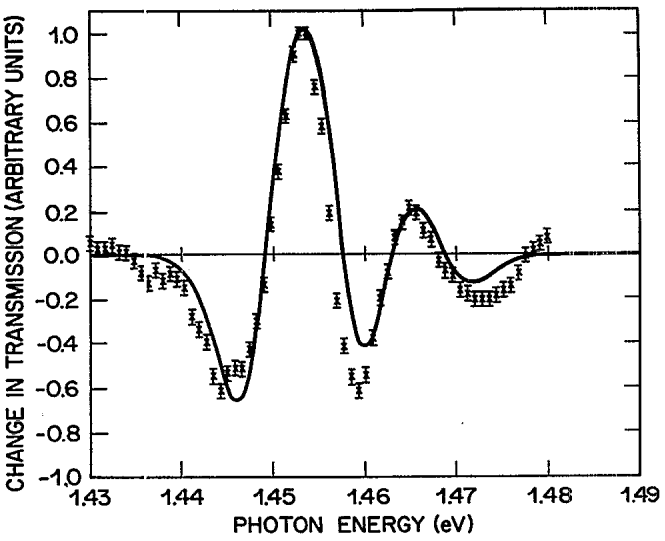

FIG. 4. Differential transmission spectrum with parallel field for 20-V applied voltage (8000 V/cm). The crosses are experimental points; the line is a semiempirical fit as discussed in the text.

B. Perpendicular field

The principal optical consequence of applying an electric field perpendicular to the quantum-well layers can be seen in Fig. 5. As increasing reverse bias is applied to the *p-i-n* diode, the whole band edge absorption shifts to lower energies, with the exciton peaks remaining resolvable, at least up to the fields shown in Fig. 5. The exciton peaks finally become unresolvable above $\approx 10^5$ V/cm. The movement of the peaks with field was measured from an extended set of spectra like those of Fig. 5. The positions of the peaks were estimated by eye from the spectra; no model was assumed for the form of the spectra (and hence no fitting procedure was used to find the peak shifts), because it is not clear "*a priori*" what effect the field inhomogeneity will have on the spectral shape, and the fields used clearly go well beyond any small signal analysis. The results of these measurements of the positions of the exciton peaks are shown by the points in Fig. 6. We also ran the *p-i-n* structure in forward bias to

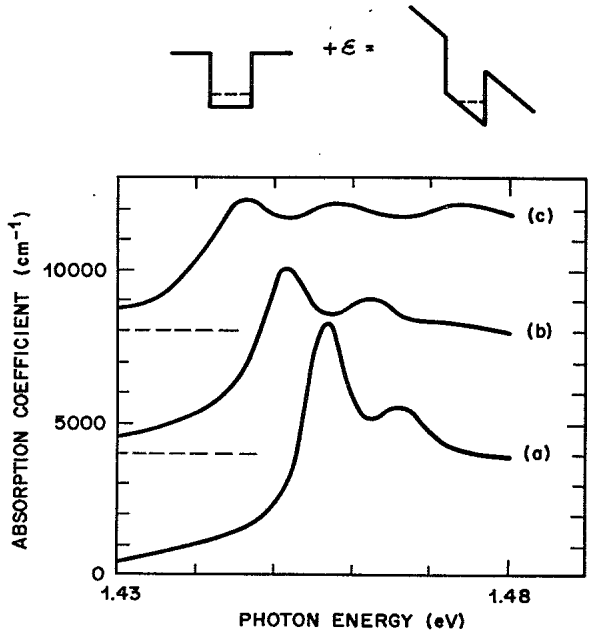

FIG. 5. Absorption spectra at various electric fields for the perpendicular field sample. (a) $\approx 1\times10^4$ V/cm; (b) $\approx 4.7\times10^4$ V/cm; (c) $\approx 7.3\times10^4$ V/cm. The insert shows schematically the distortion of the single particle quantum well potential with applied field. The zeros are displaced for clarity as shown by the dashed lines.

check that there was negligible further shift of the exciton below 10^4 V/cm. The measurement error increases from ~ 1.5 meV at low fields to ~ 4 meV at 10^5 V/cm as the peaks get broader. In general, however, the shift is clearly nonlinear, being relatively smaller for low fields. The two

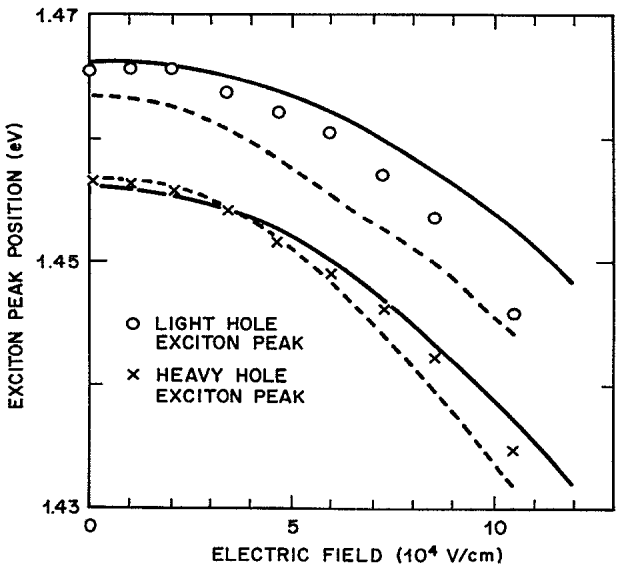

FIG. 6. Positions of the exciton peaks with applied field perpendicular to the layers. The points are experimental. The lines are theoretical calculations using the known room-temperature GaAs band gap and strain shift of the excitons, and the shifts of the exciton peaks as evaluated for the 57:43 split (solid lines) and 85:15 (dashed lines) of the band discontinuities. There are *no* fitted parameters in the theory.

excitons move at similar rates, the heavy-hole exciton energy moving more than the light-hole exciton energy. It is not possible to deduce directly from our results whether the broadening of the spectra is due to the field inhomogeneity in the sample giving different shifts for different wells or due to some other more fundamental physical cause. Because of the experimental uncertainty over broadening we also make no attempt to deduce from this data whether the area of the exciton peaks is reducing with field.

The shift of the spectrum observed in these experiments is of course approximately the same type which would be expected for a simple heating of the sample, so some care must be taken to eliminate thermal causes. There are several reasons for discounting thermal effects. First, the form of the spectra is not exactly the same as we observe on heated samples; for the degree of shift seen in our electric-field experiments (e.g., ≈ 20 meV), simple heating (e.g., by 50 K) shows much less broadening of the excitons, with the peaks remaining clearly resolved. Second, we find that we can make the changes in transmission of the sample on an *RC* time-constant-limited time scale of ≈ 2 ns (Ref. 8) when the sample is driven with a 50 Ω load. (The calculated capacitance of this sample is ≈ 20 pF.) During the 2 ns, even the total energy involved in the entire process (e.g., $\lesssim 700$ pJ for a 4 V, 2 ns pulse into a 50 Ω load) is insufficient to heat the sample by anything nearly enough to explain the observed shift; for example, 700 pJ, if totally dissipated in the 100-μm-diameter clear aperture of the device, would raise the device temperature by a calculated ≈ 0.1 K neglecting all heat conduction. This is clearly too small, as such a temperature rise would only produce ≈ 40-μeV band edge shift. Recently, we have also verified optical modulation down to 133 ps with smaller samples.[17]

The operation of this structure as a photodetector was also checked. Within experimental error we find that above 2-V reverse bias the *p-i-n* diode appears to have 100% internal quantum efficiency in the MQWS absorption region, i.e., there is one carrier pair collected for each photon absorbed in the MQWS material. A typical responsivity spectrum is shown in Fig. 7. Empirically the internal quantum efficiency is the same whether the absorption is at the exciton peaks or in the interband absorption region at higher photon energies. This is in agreement with previous discussions of the MQWS absorption at room temperature[6,10] which suggested that although absorption at the exciton peaks would initially create excitons, these would ionize into free electrons and holes on a sub- picosecond time scale by collisions with optical phonons. In fact, this ionization process has recently been time resolved directly using femtosecond laser techniques[30] implying an ionization time of ~ 300 fs.

The transport of the generated photocarriers will not be discussed in any detail in this paper. However, the observation that all the generated photocarriers are swept out of the MQWS material confirms that efficient transport does take place for both electrons and holes, despite the presence of the quantum-well barriers. A likely mechanism for this transport is thermionic emission of carriers over the barriers.[31]

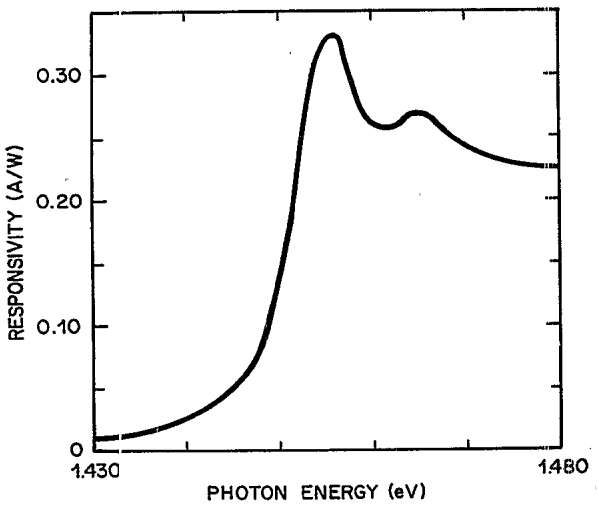

FIG. 7. Responsivity of the perpendicular-field sample (p-i-n diode) at 2-V reverse bias.

The internal quantum efficiency appears to remain $\approx 100\%$ within experimental error for all reverse bias voltages above 2 V up to ≈ 40V when avalanche gain appeared to become significant. The responsivity spectra are therefore an equally good measure of the shifts of the exciton peaks and we obtained good agreement with the transmission spectra. Our calculations from the C-V measurements show that 2 V is approximately the reverse bias for which the depletion region just extends all the way through the MQWS material. The observation that the responsivity and internal quantum efficiency fall off for reverse bias less than 2 V is also consistent with this calculation since, when the depletion region does not extend all the way through the MQWS, there will be absorption in low-field regions where the carriers may not be swept out before recombining.

It is worth pointing out here that the fact that the same MQWS material can function simultaneously as an absorptive modulator and a photodetector offers some intriguing practical applications in novel nonlinear optical devices.[18,19]

IV. THEORY AND DISCUSSION

As mentioned in the Introduction, all of the theory we will discuss will be within the effective-mass approximation. As we are considering the optical transition which creates an electron and hole, the interaction between them should be included, regardless of whether true bound electron-hole states (or excitons) exist. In fact, it has been shown[3] at least within the effective-mass approximation that the strength of the optical absorption at photon energy E is proportional to $|\psi(0)|^2$, where ψ is the solution of

$$H\psi = E\psi \tag{1}$$

with H as the effective-mass electron-hole Hamiltonian *even in the presence of electric fields.* (In fact, this remains true in the presence of any external potential, except the photon field itself.) $|\psi(0)|^2$, when properly normalized, is the probability of finding the electron and hole in the same unit cell.

We can write the Hamiltonian as

$$\begin{aligned} H = {} & H_{\mathrm{KE}z_e} + V_e(z_e) - eF_\perp z_e \\ & + H_{\mathrm{KE}z_h} + V_h(z_h) + eF_\perp z_h \\ & + H_{\mathrm{KE}reh} + V_{e\text{-}h}(\mathbf{r}, z_e, z_h) + e\mathbf{r}\cdot\mathbf{F}_{\|} , \end{aligned} \tag{2}$$

where we have the following:

(i) z_e and z_h are the coordinates perpendicular to the plane of the layer of electron and hole, respectively.

(ii) $\mathbf{r}$ is the relative position of electron and hole in the plane of the layer.

(iii)

$$H_{\mathrm{KE}z_e} = \frac{-\hbar^2}{2m^*_{e\perp}} \frac{\partial^2}{\partial z_e^2}, \quad H_{\mathrm{KE}z_h} = \frac{-\hbar^2}{2m^*_{h\perp}} \frac{\partial^2}{\partial z_h^2}$$

are the kinetic energy operators for electron and hole, respectively, in the z direction (perpendicular to the layers) with $m^*_{e\perp}$ and $m^*_{h\perp}$ being the effective masses of electron and hole, respectively, in the z direction.

(iv) $V_e(z_e)$ and $V_h(z_h)$ are the built-in rectangular quantum-well potentials for electron and hole.

(v) $F_\perp$ is the electric-field component perpendicular to the plane of the layers and $\mathbf{F}_{\|}$ is the field in the plane of the layers.

(vi)

$$H_{\mathrm{KE}reh} = \frac{-\hbar^2}{2\mu} \frac{\partial^2}{\partial \mathbf{r}^2}$$

is the kinetic energy operator of the relative motion of the electron and hole with

$$\mu = \frac{m^*_{e\|} m^*_{h\|}}{m^*_{e\|} + m^*_{h\|}}$$

being the reduced effective mass in the plane of the layers ($m^*_{e\|}$ and $m^*_{h\|}$ are the effective masses of electron and hole, respectively, in the plane of the layers).

(vii)

$$V_{e\text{-}h}(\mathbf{r}, z_e, z_h) = \frac{-e^2}{\epsilon(|z_e - z_h|^2 + r^2)^{1/2}}$$

is the Coulomb potential energy of electron and hole due to each other.

In writing the Hamiltonian H as in Eq. (2), we have already transformed the in-plane motion of electron and hole into center-of-mass coordinates using the usual transformation, and we have dropped the kinetic energy operator for center-of-mass motion; this is because we are only interested in solving for states which can be accessed optically and under optical excitation the center-of-mass motion can be neglected as the photon momentum is too small to create states of significant center-of-mass kinetic energy. Otherwise, H is a complete statement of the Hamiltonian of an electron and hole in the envelope function effective-mass approximation and the eigenvalues of H are the energies of exciton states relative to the bulk band-gap energy. In what follows we will generally only be interested in the lowest energy ($1S$-like) excitonic state. H is also the form of the Hamiltonian of any (stationary)

confined hydrogenic system, generalized here to include the different effective masses in different directions in the semiconductor. We have implicitly assumed simple constant masses m^* in defining μ above. Recent work suggests that the masses in the valence band may have a much more complicated behavior[32,33] although we will not consider this further here.

In the parallel-field case ($F_\perp = 0$) we, like previous authors,[34] will consider only the two-dimensional limit of H; here only the terms on the third line of Eq. (2) are retained, with z_e and z_h set to zero. In the perpendicular-field case ($F_\parallel = 0$) we will attempt to solve for the entire Hamiltonian of Eq. (2).

A. Parallel field

The principal conclusion from the experimental results is that the primary effect of parallel fields on the optical-absorption is to broaden the exciton resonances. Given past theoretical work on three-[3] and two-[34] dimensional excitons, this is to be expected due to field ionization shortening the exciton lifetime, and it is also in qualitative agreement with data on three-dimensional excitons in GaAs[4] where such broadening can also be resolved at room temperature in differential spectra. Several practical problems prevent a direct comparison of experiment and the prior theory. First, the experimentally accessible situation with GaAs/AlGaAs quantum wells is not near to the ideal two-dimensional limit. The excitons in our sample will have binding energies ≈ 10 meV rather than the two-dimensional limit of ≈ 17 meV ($4R_y$)[35] (the actual Rydbergs for light- and heavy-hole confined excitons are slightly different from that of the 3D case because of the slightly different hole masses in each case),[36] and the exciton diameter is correspondingly not in the two-dimensional limit either. Samples with thinner wells can be made but inhomogeneous broadening due to layer thickness fluctuations[34] and increased penetration of the wave functions into the barriers limit their usefulness in approaching a two-dimensional limit. Second, the available theories neglect any broadening mechanism for the exciton lines other than field ionization. In practice, both homogeneous broadening due to optical-phonon collisions[6,10,37] and inhomogeneous broadening due to layer thickness fluctuations[38] are both present; while the former could be reduced by cooling the latter cannot. In our sample at room temperature the two contributions are approximately equal. Third, the GaAs/AlGaAs quantum wells show two separate excitons due to the existence of light and heavy holes of different masses and consequently different confinement energies and reduced effective masses.

With these caveats, the comparison between our spectra (Fig. 3) and the theoretical spectra of Ref. 34 is qualitatively good (compare, for example, Fig. 5 of Ref. 34). Our spectra show broadening of the peaks with clearly increased absorption below and above the zero-field heavy-hole (lower energy) peak, this increase extending well above the band. Also the lowest energy peak in the absorption spectrum shifts slightly to higher energies when the broadening is strong in both our experimental results and those of the two-dimensional theory of Ref. 3. The quantitative comparison is also reasonable when the initial broadening in our data is taken into account. The field units in Ref. 34 correspond to ≈ 3 kV/cm for a two-dimensional exciton in GaAs. Therefore, spectrum (c) of Fig. 3 corresponds to 16 units; it is clearly similar to (although somewhat more severely broadened than) the spectrum for 17 units of field of Ref. 34. We should expect that the broadening should be more severe in our case compared to the two-dimensional case since the binding energy of our exciton is smaller and the exciton is larger, therefore, field ionization should require a smaller field although tunneling will take longer through the correspondingly thicker barrier in our larger exciton. Certainly when one compares two- and three-dimensional excitons, the three-dimensional one is much more readily broadened,[3] a fact that can be ascribed primarily to the lower binding energy and larger size of the three-dimensional exciton.[3]

To allow for further comparison of theory and experiment, we have fitted the differential spectrum shown in Fig. 4 semiempirically in a manner similar to that previously described.[10] The zero-field absorption is first fitted with two Gaussians (one for each exciton) and a broadened continuum; then the parameters are changed to generate differential spectra. The fit shown as the solid line in Fig. 4 corresponds to (i) broadening the heavy-hole exciton from 4.6-meV half-width at half maximum (HWHM) to 5.0-meV HWHM with 6% loss of area; (ii) broadening the light-hole exciton from 4.7-meV HWHM to 5.0-meV HWHM with no loss of area; (iii) no movement of the heavy-hole peak; (iv) movement of the light-hole peak by 0.1 meV to lower energy; (v) no change in the continuum parameters. The dominant effect appears to be broadening.

One limitation of the calculations as presented in Ref. 34 is that they do not give directly an actual field ionization rate for the exciton although their calculations do also extend to fields where such a concept is too naive. We have attempted to calculate a first approximation to this rate in Appendix A for two-dimensional excitons and to compare this with the three-dimensional case, so as to give us an alternative approach to estimating the exciton broadening. Taking a specific field such as that used for the differential spectrum of Fig. 4 (8 kV/cm) our two-dimensional model predicts a mean time to field ionization of ≈ 380 fs which would correspond to a half-width at half maximum of a simple (Lorentzian) line of 1.7 meV. Although our theory predicts a direct number for the field ionization broadening and the fit of the experimental differential spectrum yields numbers for the broadening it is not clear *a priori* how to compare the two because it is not obvious how to deconvolve the existing linewidth due to other causes. In principle, such a deconvolution can only be carried out when the physical models for the actual line shapes and their interactions are fully understood which is not the case here. The line shape of excitons in MQWS's has been studied by several authors.[6,10,38–40] The low-temperature linewidth is thought to be due to layer thickness fluctuations[38] and a Gaussian line shape has been predicted due to such inhomo-

geneities.[40] Additionally, a homogeneous broadening component, small on the low-energy side and large on the high-energy side, has been measured at low temperature and has been associated with the greater mobility of the higher-energy excitons.[39] The broadening with temperature has been measured[6,10] and is well described as optical-phonon broadening;[6,10] the linewidth at room temperature appears to be due approximately equal to phonons and inhomogeneity broadening.[6,10] The room-temperature line shape is still better described as a Gaussian rather than a Lorentzian.[10] Two simple deconvolutions are the Lorentzian case in which the linewidths Γ_A and Γ_B due to two mechanisms add linearly ($\Gamma=\Gamma_A+\Gamma_B$) and the Gaussian case in which Γ_A and Γ_B add in quadrature [$\Gamma=(\Gamma_A^2+\Gamma_B^2)^{1/2}$]. Relating HWHM Γ to lifetime τ through $\tau=\hbar/\Gamma$ we obtain $\tau=1.6$ ps for the Lorentzian deconvolution and $\tau=230$ fs for the Gaussian case for the differential spectrum measurement of the heavy-hole exciton. Clearly both of these are in order-of-magnitude agreement with the theory, although the Gaussian case is better. Moreover, it is easier to rationalize measured times shorter than the theory as the actual exciton should be easier to ionize than the extreme two-dimensional case of the theory.

The general conclusion from this comparison of theory and experiment is that the behavior of the GaAs MQWS absorption spectra near the band edge with field parallel to the layers is in good qualitative agreement with broadening due to field ionization. The quantitative comparison shows behavior much closer to the two-dimensional limit than the three-dimensional limit with the excitons apparently taking much longer to field ionize than would a three-dimensional exciton.

B. Perpendicular fields

The experimental results (Figs. 5 and 6) show that a strong effect of the electric field perpendicular to the quantum-well layers on the optical absorption near the band gap is to shift the absorption to longer wavelengths (lower photon energies). Although there may be some broadening of the absorption, it is apparently much less than that seen at comparable fields in the parallel direction; with parallel fields the exciton peaks are unresolvable by $\approx 1.6\times10^4$ V/cm whereas the peaks are resolvable up to $\approx 10^5$ V/cm for perpendicular fields. We will attempt to model the shifts in energy of the exciton peak with field and to explain this remarkable persistence of the peaks to very high fields.

Various parts of the Hamiltonian of Eq. (2) have already been treated separately. First we consider the zero-field parts. $H_{\mathrm{KE}z_e}+V_e(z_e)$ (and the equivalent for holes) is just the Hamiltonian of a particle in a one-dimensional rectangular potential well and the solutions of this are well known.[41] One complication in actually solving these "particle-in-a-box" problems for the GaAs/AlGaAs system is the relative size of V_e and V_h. Until recently, it was believed that the discontinuity in the band gap at the GaAs/AlGaAs interface was split 85:15 (Ref. 41) between conduction (V_e) and valence (V_h) bands. However, recently there has been considerable evidence that the split is more even.[42–46] Most of these results suggest a split ratio within a few percent of 60:40 (Refs. 42—44 and 46). We will consequently do all our calculations for both 85:15 and 57:43 (Ref. 42) split ratios (see Table I).

TABLE I. Effective masses and well potentials for 85:15 and 57:43 conduction: valence potential ratios as used for calculations. x is the aluminum mole fraction.

	85:15	57:43
m_e^*	$0.0665+0.0835x$	$0.0665+0.0835x$
m_{h-h}^*	$0.45+0.31x$	$0.34+0.42x$
m_{l-h}^*	$0.088+0.049x$	$0.094+0.043x$
V_e (meV)	340	228
V_h (meV)	60	172

With a finite field applied perpendicular to the wells, several approaches can be taken to solve for the effect on the individual particle-in-a-box energies [i.e., the Hamiltonian $H_{\mathrm{KE}z_e}+V_e(z_e)-eF_\perp z_e$ and the equivalent for holes]. Variational methods have been used[26] for both finite and infinite wells with simple solutions for the infinite-well case. In Appendix B of this paper we solve exactly for the infinite-well case; the resulting wave functions are Airy functions. In Appendix C of this paper we solve numerically using a tunneling resonance method for a particular finite well designed to model the conditions in our sample. The comparison between these various models is interesting. We find as discussed in Appendix B that the variational model for infinite wells is remarkably close in the calculated energies to the exact Airy function model. Infinite-well models using the true physical thicknesses do not model the behavior with field well quantitatively when compared to the numerical model in Appendix C; this can at least in part be attributed to the fact that such an infinite-well model is not a good model even at zero field because the energies of the first confined states are significantly different from the infinite-well results. However, we find that if we use effective widths, $L_{\mathrm{eff}e}$, $L_{\mathrm{eff}h\text{-}h}$, and $L_{\mathrm{eff}l\text{-}h}$ (for electron, heavy hole, and light hole, respectively) for infinite wells so that we obtain the correct zero-field energies, then we obtain remarkably good agreement between the tunneling resonance numerical calculations and this effective infinite-well model. The effective widths used are given in Table II. This comparison is made in greater detail in Appendix C. Of course, the effective widths, L_{eff}, which are all greater than the physical widths, are different for electron, heavy hole, and light hole. However, this larger effective width merely approximates the fact that there is significant penetration of the wave functions into the barriers. The

TABLE II. Effective infinite-well widths used when calculating finite-well properties with infinite-well models.

	85:15 (Å)	57:43 (Å)
$L_{\mathrm{eff}e}$	126	133
$L_{\mathrm{eff}h\text{-}h}$	121	114
$L_{\mathrm{eff}h}$	155	129

important physical insight derived from this effective-well-width model is that as far as these perpendicular electric field shifts are concerned the primary consequence of finite wells is simply to make the wave function larger; this might not seem so remarkable were it not for the fact that this remains true up to $\approx 10^5$ V/cm where the electric potential drop across the wells is ≈ 100 meV, considerably larger than the confinement energies of any of the states at zero field and comparable to or greater than the zero-field well depths.

This comparison of the various models therefore shows that in practice we may use any of them to obtain a reasonable approximation to the behavior of the particle-in-a-box levels as the box becomes skewed by applied field provided only that the appropriate effective widths are used for the infinite-well models. The tunneling resonance calculations of the shifts of the single-particle states are summarized in Fig. 8(a). For the detailed comparison of the various calculations of single-particle energy shifts, see Appendices B and C.

Now we consider the effects of electron-hole interaction;

$$H_{\mathrm{KE}reh}+V_{e\text{-}h}(\mathbf{r},z_e,z_h)+H_{\mathrm{KE}z_e}+V_e(z_e)+H_{\mathrm{KE}z_h}+V_h(z_h)$$

is the Hamiltonian of the electron-hole system with no field in a rectangular potential well. By solving for the eigenvalues of this Hamiltonian and subtracting the one-dimensional particle-in-a-box energies of the separate particles, the zero-field binding energy of the exciton can be calculated. This has been attempted variationally,[36,47–49] perturbatively[50] adiabatically,[51] and using a combined variational-perturbative technique.[52]

Now we will attempt to evaluate all of the terms in H simultaneously. There is one obvious physical effect (contained in H) which, as yet, has not been addressed; specifically, as the field is applied, electrons and holes move to opposite sides of the quantum wells and as a consequence the Coulomb attraction between electron and hole is reduced, reducing the binding energy of the exciton and thereby acting to increase the energy of the exciton resonance. To attempt full solution of Eq. (2), we will use a variational method with the separable trial function,

$$\Psi(\mathbf{r},z_e,z_h)=\psi_e(z_e)\psi_h(z_h)\phi_{e\text{-}h}(\mathbf{r}) , \tag{3}$$

where $\psi_e(z_e)$ and $\psi_h(z_h)$ are the "exact" wave functions of the individual electrons and holes in the one-dimensional quantum wells with an applied field [i.e., the lowest eigenfunctions of $H_{\mathrm{KE}z_e}+V_e(z_e)-eF_\perp z_e$ and the equivalent for holes] and

$$\phi_{e\text{-}h}(\mathbf{r})=\left[\frac{2}{\pi}\right]^{1/2}\frac{1}{\lambda}\exp\left[\frac{-r}{\lambda}\right]$$

(i.e., we choose a simple $1S$-like orbital for the in-plane radial motion) with λ, the amplitude radius of the exciton orbit, as an adjustable parameter. This wave function is probably about the simplest that can be chosen while still preserving the principle features of the actual wave function; the separability makes the whole problem much more tractable. This wave function is not valid for wells comparable to or thicker than the three-dimensional exciton diameter (~ 300 Å) as it does not tend to the three-dimensional wave function in the limit. However, it is a good approximation for the thin wells (~ 100 Å) used here as can be checked "*a posteriori*" by evaluating the zero-field binding energy and comparing the result with other methods. This wave function will also include effects of finite-well depth.

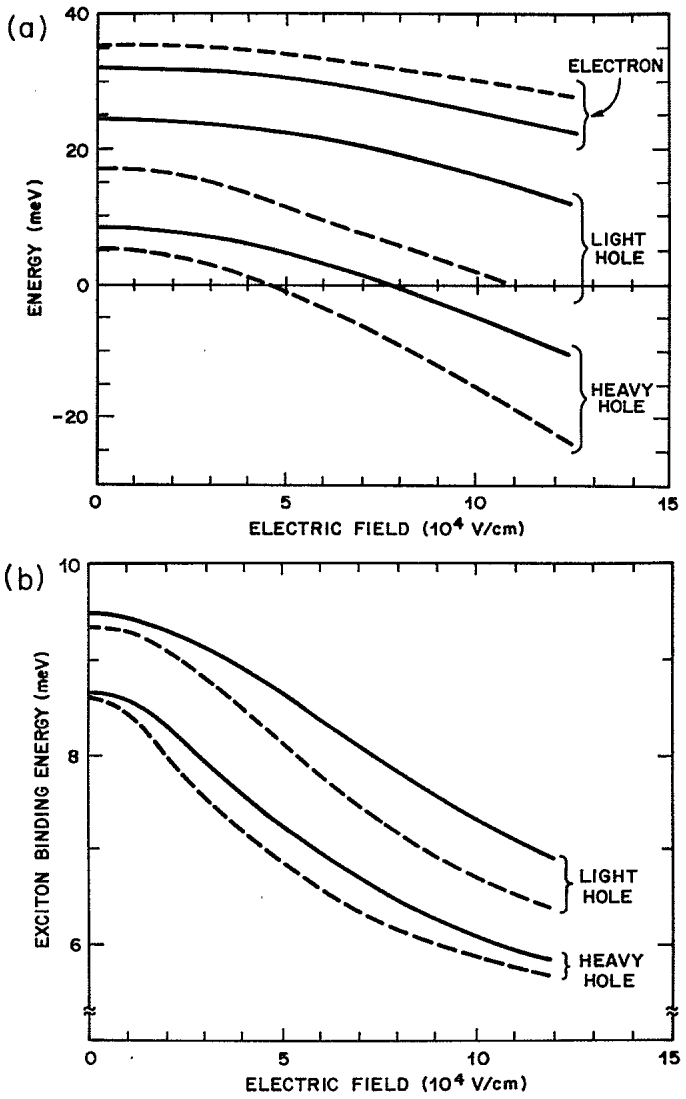

FIG. 8. (a) Energies of the first electron, heavy-hole, and light-hole states relative to the potentials at the center of the quantum well as calculated using the tunneling resonance method (Appendix C). (b) Exciton binding energy (Ref. 53) contribution E_B as calculated variationally in Appendix D. The solids lines use the 57:43 discontinuity split and the dashed lines use the 85:15 split. The final exciton energy is calculated by adding the appropriate hole energy, the electron energy and the band-gap energy, and subtracting the exciton binding energy; the light-hole energy also has a fixed strain shift to be added (see the text).

Formally evaluating the expectation value of H we obtain

$$\langle\Psi\,|\,H\,|\,\Psi\rangle=E_e+E_h+E_B , \tag{4}$$

where E_e and E_h are the energies of the individual elec-

trons and holes already evaluated and E_B, which we will refer to here as the exciton binding energy,[53] is given by

$$E_B = E_{\mathrm{KE}r} + E_{\mathrm{PE}r} , \tag{5}$$

where $E_{\mathrm{KE}r}$, the kinetic energy of relative electron-hole motion in the layer plane is given by

$$E_{\mathrm{KE}r} = \langle \phi_{e\text{-}h} \mid H_{\mathrm{KE}reh} \mid \phi_{e\text{-}h} \rangle = \frac{\hbar^2}{2\mu\lambda^2} , \tag{6}$$

and $E_{\mathrm{PE}r}$, the Coulomb potential energy of the electron-hole relative motion, is given by

$$E_{\mathrm{PE}r} = \langle \Psi \mid V_{e\text{-}h} \mid \Psi \rangle . \tag{7}$$

$E_{\mathrm{PE}r}$ is also of course dependent on the variational parameter λ. The evaluation of the integrals in Eq. (7) is not straightforward. The fact that the wave function Ψ is separable is of less use here because the potential $V_{e\text{-}h}$ couples all the variables. However, this can be integrated partly analytically and partly numerically and the details of this and the variational minimization of the resulting E_B are discussed in Appendix D. For the calculation of $E_{\mathrm{PE}r}$, we actually use the variational wave functions[26] of the infinite well for $\psi_e(z_e)$ and $\psi_h(z_h)$ as there are no analytic wave functions available from the tunneling resonance calculation and the variational wave functions are much simpler to use than the Airy functions of the exact infinite-well solution in Appendix B; the discussion above showed that all three methods are in good agreement provided that the correct effective well widths L_{eff} are used. The resulting calculations of the shift in exciton binding energy are shown in Fig. 8(b).

One further energy is required before making the comparison with experiment, namely, the strain shift of the light-hole exciton peak. For our sample, we calculate using the data of Dingle and Wiegmann[54] that the built-in strain in the sample will shift the light-hole exciton to lower energy by 4.5 meV. Finally, using the room-temperature band-gap energy 1.424 (Ref. 55) and adding the calculations in Fig. 8 (together with the strain shift) we obtain the solid line shown in Fig. 6 for the 57:43 split calculations; this fit has *no adjustable parameters* and the energies are in absolute values, not relative shifts. The discrepancy between the light-hole exciton peak shift and the theory is well within the width of the light-hole peak as can be seen from Fig. 5. Therefore, we have excellent agreement between experiment and theory for the positions of the exciton peaks with field. The 85:15 split (dashed lines in Fig. 6) gives nearly as good a fit, although there is a discrepancy of 2 meV in the zero-field position of the excitons.

The fact that the 57:43 and 85:15 split ratios give very similar overall shifts for the exciton peaks is surprising in view of the very different single particle shifts in each case [Fig. 8(a)]. Apparently, the sum of electron and hole energies is approximately equal for the two split ratios even though the individual energies are significantly different. This compensation makes the exciton energy insensitive to split ratio even with strong fields. The zero-field binding energies for the excitons are incidentally in good agreement with other calculations which use more sophisticated wave functions;[36,48,49,52] this therefore provides further justification for the use of the simple wave function of Eq. (3).

It is apparent from Fig. 8 that the dominant contribution to the exciton shift at high fields is the shift of the particle-in-a-box energies of the individual electron and holes E_e and E_h. The dominance of the shifts of E_e and E_h at high fields comes about because the shift of exciton binding energy E_B saturates out somewhat at high fields as is discussed in Appendix D. However, at low fields (e.g., $\lesssim 3\times10^4$ V/cm), the effect of the shift of E_B is very important as it can reduce the shift of the exciton peaks by factors ≈ 2; our experiments are not, however, particularly sensitive at these fields.

Thus far, we have shown that we can explain the magnitude of the shift of the exciton peaks with field very accurately for the perpendicular fields. However, we have not yet addressed why it is that we can still observe exciton peaks in the perpendicular-field case at fields which correspond to ~ 50 times the classical ionization field of a three-dimensional exciton of comparable binding energy, with associated shifts ~ 2.5 times the zero-field binding energy; by contrast in the parallel-field experiments the excitons disappear at a few times the ionization field and the shift is $\lesssim 10\%$. To understand this persistence of the peaks, we must reexamine why it is that the exciton peaks normally broaden with field. As discussed in the introduction, the broadening essentially results from the rapid field ionization of electron and hole, or, equivalently, the tunneling of electron and hole away from one another.

There are two separate processes which are relevant in considering this tunneling for the quantum-well structures. First, the electron and hole tend to separate within one well when the perpendicular field is applied; the electron moves towards one wall and the hole moves towards the other. This reduces the Coulomb energy of the electron and hole. Our binding energy calculations show, however, that the exciton is still strongly bound even at high fields (e.g., 6—7 meV at 10^5 V/cm). This is because the well is thin (e.g., 100 Å) compared to the 3D exciton diameter (e.g., 300 Å). If the well was thick (e.g., 1000 Å) compared to the 3D exciton diameter, then the electron and hole could tunnel through the Coulomb potential barrier which binds the exciton, resulting in a state with the electron and hole separated to opposite sides of the well with very little Coulomb interaction between electron and hole and the exciton would be effectively field ionized; in this extreme situation, the absorption spectra would be essentially those of the 3D system. Of course, the walls of the wells only inhibit the field ionization if the individual electrons and holes do not tunnel rapidly through the walls of the wells, i.e., through the heterostructure barriers. A simple way to estimate the strength of this second tunneling process is to estimate the rate of tunneling of an individual electron or hole out of the well (i.e., through the heterostructure barrier). This is a slight overestimate of the actual field ionization rate as it neglects the additional confining effect of the Coulomb attraction of electron and hole, although usually this attraction is small compared to the confinement due to the heterostructure for the fields we use here. We can deduce

this single-particle tunneling rate from the widths of the tunneling resonances of the single-particle states; if the resonance has a half-width at half maximum of ΔE, then the lifetime of a particle in the state is $\sim\hbar/\Delta E$. The resonance widths as calculated from the tunneling resonance method of Appendix C are shown in Fig. 9. The 85:15 split shows comparatively strong tunneling for the holes as would be expected due to the shallow valence-band well in this case. However, even these 85:15 split hole level widths are consistent with the data, as the resonances just become experimentally unresolvable at $\sim 10^5$ V/cm which is where the light-hole tunneling resonance width becomes comparable with the binding energy. Of course there are other sources of broadening (such as, apparent broadening due to the field inhomogeneity in the quantum wells) and so this data should not be taken as evidence for the 85:15 split; the point is rather that even the most pessimistic calculation confirms that the tunneling of the individual particles out of the wells is not sufficiently strong to destroy the exciton resonances at the fields used here. Hence, we can conclude that the consequences of (i) (quantum) confinement of the exciton within much less than the bulk exciton diameter and (ii) inhibition of electron and hole motion by the heterojunction potential barriers, inhibit the field ionization of the exciton, allowing it to exist to very high fields.

As mentioned before, the Hamiltonian Eq. (2) is basically that of a hydrogenic system with a confining potential in one direction and an applied electric field. The shift in the energy of the system with field can therefore be viewed as a Stark shift. However, it is clear from our experiments and theory that the quantum confinement leads to qualitatively different phenomena (i.e., persistence of resonances to high fields and very large resonance shifts). Hence, we have called this perpendicular-field electroabsorption the quantum-confined Stark effect.[20] In principle, it should also be observable in other hydrogenic systems, although the fields required to observe it in actual hydrogen atoms are not readily accessible experimentally.

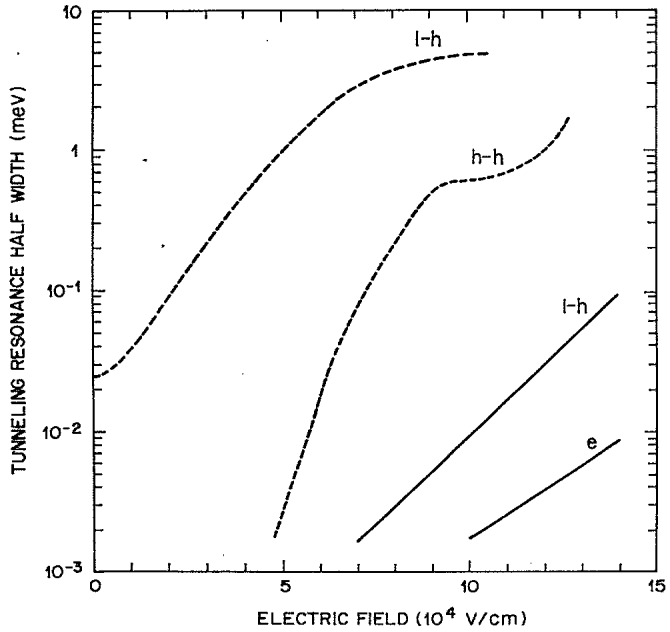

FIG. 9. Half widths at half maximum of the tunneling resonances as a function of the field. Solid lines, 57:43 split. Dashed lines, 85:15 split. *e* represents the first confined electron level; *l-h* and *h-h* represent the first confined levels of light hole and heavy hole, respectively. The electron in the 85:15 split and the heavy hole in the 57:43 split have half-widths less than 1 μeV for all fields shown here. At fields above $\sim 6\times 10^4$ V/cm, the light-hole resonance for the 85:15 split becomes asymmetric; we use the smaller of the two half-widths, corresponding to the low-energy side of the resonance. The half-width on the high-energy side becomes undefined because of a rising background tunneling current.

V. CONCLUSIONS

We have investigated the dependence of band edge optical absorption in GaAs/AlGaAs quantum-well structures. We find distinct effects for fields parallel and perpendicular to the quantum-well layers.

For parallel fields, we find that the band edge absorption broadens with increasing field in a manner at least qualitatively consistent with field ionization (Stark broadening). Detailed quantitative agreement with theory is not possible, but order-of-magnitude agreement is found.

For perpendicular fields, we find that the absorption edge shifts to lower photon energies with increasing field; the exciton peaks remain resolved at up to 50 times the classical ionization field and shifts as large as 2.5 times the zero-field binding energy are found. The shifts are explained very well without any fitted parameters by theory which treats the entire Hamiltonian of the exciton in the quantum well in the effective-mass approximation. The explanation of the persistence of the peaks to such high fields is that (i) the field ionization is impeded because the individual electrons and holes do not tunnel rapidly out of the wells and (ii) even when the electron and hole are substantially pulled to opposite walls of the well by the field, the Coulombic binding of electron and hole is still strong because the well thickness is small compared to the three-dimensional exciton diameter. This mechanism truly requires quantum confinement of carriers in thin layers; as such it is distinct from the Franz-Keldysh effect of bulk semiconductors. Because the theoretical formalism is simply that of an electric field applied to a confined hydrogenic system we refer to this mechanism as the quantum-confined Stark effect.

Although reported here for only one physical system we expect the physical effects to be applicable to other layered semiconductor systems and more generally to other confined hydrogenic systems; in this regard the GaAs/AlGaAs quantum-well system has proven to be an excellent physical testing ground for the physics of confined hydrogenic systems in very high fields.

APPENDIX A: FIELD IONIZATION FOR A TWO-DIMENSIONAL EXCITON

The problem of an hydrogen atom whose motion is restricted to a plane but with particles still interacting through the $1/r$ Coulomb potential, can be solved exact-

ly.[56–58] It is found that the ground-state energy and wave function are

$$E_{1S}=-4R_y,\quad \Psi_{1S}=\left[\frac{2}{\pi}\right]^{1/2}\frac{2}{a_0}\exp(-2r/a_0)\,,$$

where the Rydberg energy and Bohr radius are $R_y=\mu e^4/2\hbar^2\epsilon^2$ and $a_0=\epsilon\hbar^2/e^2\mu$. A detailed discussion of two-dimensional excitons is found in Ref. 35. The analysis of the effect of a static field on such a system can be transposed directly from the well-documented case of a three-dimensional hydrogen atom.[59,60] In this appendix we will use the atomic units which are a_0 for the lengths, $E_0=2R_y$ for the energies E, and $F_0=E_0/ea_0$ for the fields $F_{||}$. We choose the y axis along the direction of the field and, to separate the variables, we use two-dimensional parabolic coordinates: $x=\sqrt{\xi\eta}$, $y=\frac{1}{2}(\xi-\eta)$, and $r=\frac{1}{2}(\xi+\eta)$. The Schrödinger equation in normal units is

$$\left[-\frac{\hbar^2}{2\mu}\nabla^2-\frac{e^2}{\epsilon r}-eF_{||}y\right]\psi=E\psi$$

and in a.u. with $f_{||}=F_{||}/F_0$,

$$\left[\nabla^2+2\left[E+\frac{1}{r}+f_{||}y\right]\right]\Psi=0\,.$$

For the ground state, i.e., $E_{1S}=-4R_y$ it transforms in parabolic coordinates to

$$\frac{4}{\xi+\eta}\left[\xi\frac{\partial^2}{\partial\xi^2}+\frac{1}{2}\frac{\partial}{\partial\xi}+\eta\frac{\partial^2}{\partial\eta^2}+\frac{1}{2}\frac{\partial}{\partial\eta}\right]\Psi + \left[-4+\frac{4}{\xi+\eta}+f_{||}(\xi-\eta)\right]\Psi=0\,. \quad \text{(A1)}$$

Taking for the wave function the form

$$\Psi=\xi^{-1/4}g_+(\xi)\eta^{-1/4}g_-(\eta)\,, \quad \text{(A2)}$$

it is found that $g_+(\xi)$ and $g_-(\eta)$ are solutions of one-dimensional Schrödinger equations

$$\left[\frac{d^2}{d\xi^2}-1+\frac{1}{2\xi}+\frac{3}{16\xi^2}-\frac{1}{4}f_{||}\xi\right]g_+(\xi)=0\,, \quad \text{(A3a)}$$

$$\left[\frac{d^2}{d\eta^2}-1+\frac{1}{2\eta}+\frac{3}{16\eta^2}+\frac{1}{4}f_{||}\eta\right]g_-(\eta)=0\,. \quad \text{(A3b)}$$

These equations can be interpreted as describing the one-dimensional motions of two independent particles, one moving on the potential

$$u_+=-\frac{1}{2\xi}-\frac{3}{16\xi^2}+\frac{1}{4}f_{||}\xi$$

and the other in the potential

$$u_-=-\frac{1}{2\eta}-\frac{3}{16\eta^2}-\frac{1}{4}f_{||}\eta\,.$$

The former is always bounded and only the latter can field ionize. The wave function outside the potential well is connected to the wave function inside the well by the usual technique.[60] Using inside the well the unperturbed wave function

$$\Psi=\frac{4}{\sqrt{2\pi}}\exp[-(\xi+\eta)]\,,$$

and

$$g_{\text{out}}\simeq g_{\text{in}}\left[\frac{|p_0|}{p}\right]^{1/2}\exp\left[i\int_{\eta_0}^{\eta}p\,d\eta-\frac{i\pi}{4}\right], \quad \text{(A4)}$$

where

$$p=\left[-1+\frac{1}{2\eta}+\frac{3}{16\eta^2}+\frac{1}{4}f_{||}\eta\right]^{1/2},$$

the ionization rate is found by calculating the probability current in the y direction, i.e.,

$$\omega=\int_0^{\infty}|\psi|^2v_y dx\,. \quad \text{(A5)}$$

The broadening induced by the field is $\Gamma\equiv\hbar\omega$:

$$\frac{\Gamma_{2D}}{R_y}=\frac{64}{\sqrt{\pi}}\left[\frac{R_y}{eF_{||}a_0}\right]^{1/2}\exp\left[-\frac{32R_y}{3eF_{||}a_0}\right] \quad \text{(A6)}$$

compared to the three-dimensional result[60]

$$\frac{\Gamma_{3D}}{R_y}=16\left[\frac{R_y}{eF_{||}a_0}\right]\exp\left[-\frac{4R_y}{3eF_{||}a_0}\right], \quad \text{(A7)}$$

where for clarity we have returned to the usual units.

We see that the field induced broadening is smaller in 2D not only because of the increased energy of the ground state but also because the reduced dimensionality modifies the first term functional form, from $F_{||}^{-1}$ in 3D to $F_{||}^{-1/2}$ in 2D. In Fig. 10 we have plotted the field-induced broadenings for 2D and 3D excitons using the GaAs parameters, i.e., $R_y=4.2$ meV, $a_0=140$ Å.

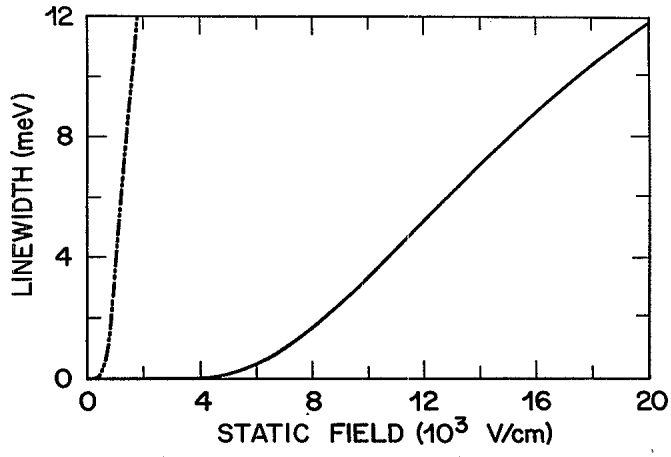

FIG. 10. Linewidth contribution Γ for two-dimensional (solid line) and three-dimensional (dashed line) excitons due to field ionization by a static electric field as calculated in Appendix A.

APPENDIX B: EXACT SOLUTION FOR A PARTICLE IN AN INFINITE WELL IN THE PRESENCE OF A UNIFORM STATIC FIELD

The problem of a charged particle in a uniform static field has been considered in a number of articles[61–63] and text books.[60] It is found that if in addition the particle is restrained to stay within an infinitely deep well, an exact solution can be obtained for any value of the static field. This is a consequence of the very simple and severe boundary conditions imposed upon the wave function $\zeta(z)$, i.e., $\zeta(\pm\frac{1}{2}L_z)=0$ for any field. The Schrödinger equation can be written

$$-\frac{\hbar^2}{2m^*}\frac{d^2}{dz^2}\zeta(z)-(W+eF_\perp z)\zeta(z)=0\ . \tag{B1}$$

The zero-field solutions are known, i.e.,

$$W_n=\frac{\hbar^2}{2m^*}\left[n\frac{\pi}{L_z}\right]^2, \tag{B2a}$$

$$\zeta_n(z)=\left[\frac{2}{L_z}\right]^{1/2}\cos\left[n\frac{\pi}{L_z}z\right]\ . \tag{B2b}$$

It is therefore natural to use as the unit of energy the energy of the ground state

$$W_1=\frac{\hbar^2}{2m^*}\left[\frac{\pi}{L_z}\right]^2$$

and as the unit of field F_1 such that $eF_1L_z=W_1$.

In order to transform Eq. (B1) into the Airy differential equation it is convenient to use the new variable Z:

$$Z=-\left[\frac{2m^*}{(e\hbar F_\perp)^2}\right]^{1/3}(W+eF_\perp z)\ . \tag{B3}$$

Note that $W+eF_\perp z$ represents the kinetic energy and that $[(e\hbar F_\perp)^2/2m^*]^{1/3}$ has the dimensions of an energy. Z is therefore a normalized kinetic energy. The new form of Eq. (B1) is written

$$\frac{d^2}{dZ^2}\zeta(Z)-Z\zeta(Z)=0 \tag{B4}$$

whose solutions are of the form

$$\zeta(Z)=a\,\mathrm{Ai}(Z)+b\,\mathrm{Bi}(Z)\ , \tag{B5}$$

where a and b are two constants and Ai(Z) and Bi(Z) are the Airy functions.[64] The boundary conditions are

$$\zeta(Z_+)=\zeta(Z_-)=0\ ,$$

where $Z_\pm=Z(\pm\frac{1}{2}L_z)$. If we measure the energies and field in units W_1 and F_1, i.e.,

$$w=\frac{W}{W_1},\quad f=\frac{F_\perp}{F_1}\ ,$$

then

$$Z_\pm=\left[-\frac{\pi}{f}\right]^{2/3}(w\pm\tfrac{1}{2}f) \tag{B6}$$

and

$$0=\mathrm{Ai}(Z_+)\mathrm{Bi}(Z_-)-\mathrm{Ai}(Z_-)\mathrm{Bi}(Z_+)\ , \tag{B7}$$

which completely determines the eigen energy. Note that in the normalized form the effective mass and the well thickness have disappeared. Equations (B6) and (B7) are therefore universal. Two limits are easily analyzed using the asymptotic forms of Ai(Z) and Bi(Z).[64] For $F\to 0$ one finds $w^2=n^2$ in agreement with Eq. (B2a). For $F_\perp\to\infty$ one finds $w\to\mp\frac{1}{2}f+[\frac{3}{2}(n-\frac{1}{4})f]^{2/3}$ with $n\gg 1$. For other values of $F_\perp$, Eq. (B7) can be solved numerically to the desired accuracy using the series expansion of the Airy functions.[64] The universal curve $w(f)$ obtained by this method is given in Fig. 11. For comparison we have extended the infinite-well variational calculations of Ref. 14 to higher energies and plotted these also in Fig. 11. It can be seen that the variational method also remains accurate up to very large fields.

APPENDIX C: TUNNELING RESONANCE CALCULATIONS OF ENERGY LEVELS AND LEVEL WIDTHS IN A FINITE WELL WITH APPLIED ELECTRIC FIELD

In this appendix, the energies of the electron and hole states in quantum wells with an applied field perpendicular to the wells are calculated by an exact computer solution of the Schrödinger equation in the effective-mass approximation for particle transmission through the quantum-well potentials.[65] We also calculate the widths of these resonances to deduce the broadening due to particles tunneling out of the wells. The electron or hole energies in the GaAs quantum well are computed by calculating the transmission of electrons or holes through a well and two barriers as shown in Fig. 12. At energies of the quantum-well bound states, the particle transmission is maximum. The positions of the particle transmission resonances thus identify the quantum-well energies. The

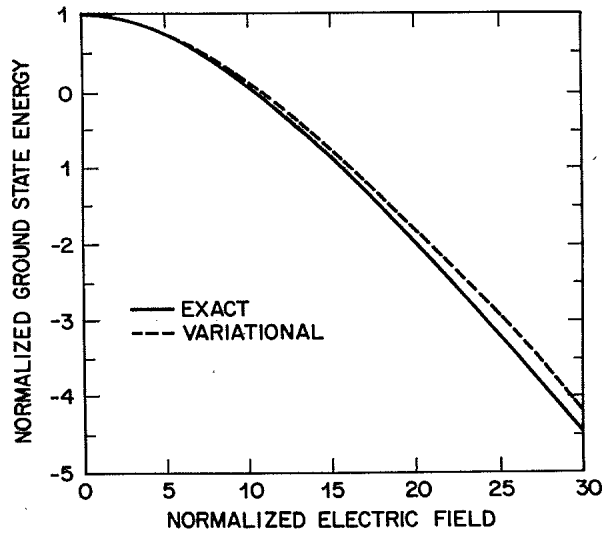

FIG. 11. Universal curve for the energy of the first state in an infinite quantum well in the presence of a uniform electric field perpendicular to the walls of the well. Solid curve is the exact solution. Dashed curve is the variational calculation (Ref. 26).

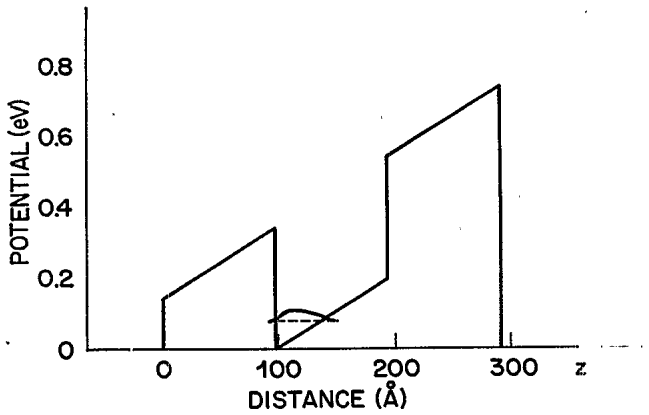

FIG. 12. Potential profile used in particle transmission (tunneling resonance) calculation of electron and hole quantum-well energies, shown here for electrons in a field of 2.06×10^4 V/cm (600 meV across one well and two barriers) for the 85:15 split.

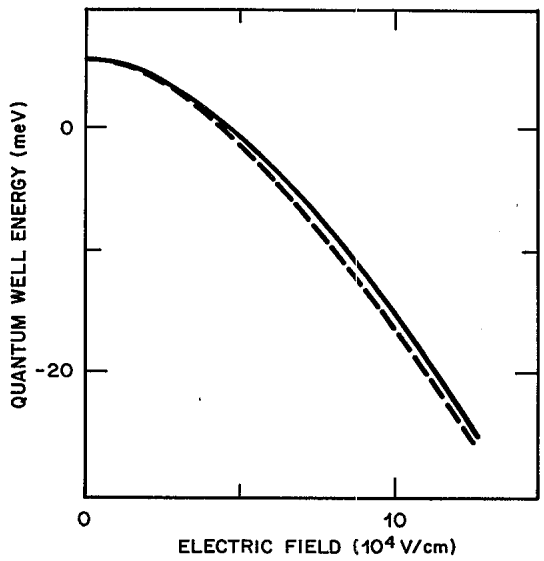

FIG. 13. Comparison of the tunneling resonance calculation (solid line) and exact infinite-well calculation with appropriate effective-well width (dashed line) for the extreme case of the heavy-hole energy level for the 85:15 band-gap discontinuity split.

electrons and holes in an electric field are, in fact, quasibound, and the strength and width of the resonances indicate the lifetimes of the particles.

We have performed the calculations for two sets of parameters, one for the 85:15 split of the conduction- and valence-band discontinuities and the other for the 57:43 (Ref. 42) split. Different masses are appropriate in each case; the masses are those which allow best fits to zero-field absorption spectra in each case. We summarize the parameters in Table I. V_e and V_h are the actual discontinuities at the interfaces.

The Al content, x, is zero in the GaAs well and $x=0.32$ in the $Al_xGa_{1-x}As$ barrier. The potential for the 95 Å quantum well with 98 Å barriers is represented in the calculation as a series of 30 steps in the well and 20 steps in the barriers. The form of the model potential is shown in Fig. 12; this is an approximation to the real potential of the multiple well system, but it includes the major consequences of the first finite barriers around a given well. The field extends through both barriers and the well and is constant throughout. The band-gap difference between GaAs and $Al_xGa_{1-x}As$ is taken as $1.425x-0.90x^2+1.1x^3$.

The energies of the electron, heavy-hole, and light-hole states with respect to the potentials at the center of the quantum well are shown as a function of applied field in Fig. 8. The $n=1$ electron level shifts superlinearly with electric field. In the 85:15 case the heavy-hole and light-hole levels shift strongly but become broad at high fields as their energies approach the energy of the lower confining barrier and they become less confined (see Fig. 9). In the 57:43 case, the shifts are more equal although the sum of electron and hole shifts is very close to that of the 85:15 split. The stronger shifts for the holes in the 85:15 case result from the high mass of heavy holes and the strong penetration of the relatively low hole barrier by the light holes. In the 57:43 case the broadening is very small at all fields accessed experimentally (see Fig. 9). In both cases, tunneling between wells produces negligible shifts with the present barrier thicknesses.

The tunneling resonance widths for the extreme case of the 85:15 split also show some other incidental features. The light-hole resonance on the 85:15 split shows a finite width at zero field; this is presumably the start of the superlattice bandwidth, although the model used here does not include true superlattice effects as only one well and two barriers are considered. Another way of expressing this is to say that tunneling of the light hole between wells at zero field is significant on this scale. The kink in the HWHM near 10^5 V/cm for the heavy-hole resonance in the 85:15 split calculation is not itself important for our conclusions but is physically intriguing. At these fields, the barrier seen by the holes on one side is essentially triangular, with the width being simply dependent on field. One possible explanation for the kink is the formation of a resonance due to the reflection off the far (sloping) side of the barrier interfering constructively with the wave function inside the well; such a resonance tends to confine the particle increasing the time before it tunnels completely out of the well and tending to reduce its resonance width.

In Fig. 13, we compare the results of two models: (i) the tunneling resonance finite-well model and (ii) the exact infinite-well model using the effective infinite-well-width approximation, both for the rather extreme case of the heavy-hole level shift with the 85:15 split. As can be seen, both methods agree remarkably well. The variational infinite-well model with effective-well widths also agrees with both of these models within the same accuracy (see Fig. 11). We presume that the tunneling resonance calculation is best as it most completely includes the effects of finite wells. However, the good agreement justifies the use of the effective finite-well approximation for the calculation of the exciton binding in Appendix D.

APPENDIX D: EXCITON BINDING ENERGY WITH STATIC FIELDS PERPENDICULAR TO THE LAYERS

The evaluation of the binding energy of an exciton in a quantum well with an electric field perpendicular to the quantum-well layers has been discussed in general terms in Sec. IV, where the rationale behind the present method has been discussed. The most difficult part of the variational calculation is the evaluation of the potential energy, E_{PE}, as defined in Eq. (7). Written explicitly this becomes

$$E_{\mathrm{PE}}=\frac{-2e^2}{\pi\epsilon\lambda^2}N^2(\beta_e)N^2(\beta_h)\int_{\theta=0}^{2\pi}\int_{r=0}^{\infty}\int_{z_e=-L_e/2}^{+L_e/2}\int_{z_h=-L_h/2}^{+L_h/2}\cos^2\frac{\pi z_e}{L_e}\exp\left[-2\beta_e\left[\frac{z_e}{L_e}+\frac{1}{2}\right]\right]$$
$$\times\cos^2\frac{\pi z_h}{L_h}\exp\left[-2\beta_h\left[\frac{z_h}{L_h}+\frac{1}{2}\right]\right]$$
$$\times\frac{r\exp(-2r/\lambda)}{[(z_e-z_h)^2+r^2]^{1/2}}d\theta\,dr\,dz_e\,dz_h\ . \tag{D1}$$

Here, we have used the variational wave functions for electron and hole[26] as discussed in Appendix B and Sec. IV because they are analytically simple and give the correct energies for electron and hole states provided we use the effective-well widths appropriate for the wells in question. These are different for each electron and hole and for each of the two splits of the band discontinuity (85:15 and 57:43); the effective widths used are given in Table II. The normalization factors of the electron and hole wave functions are

$$N^2(\beta)=\frac{4\beta}{L[1-\exp(-2\beta)]}\frac{\beta^2+\pi^2}{\beta^2},$$

where L is the appropriate effective-well width.

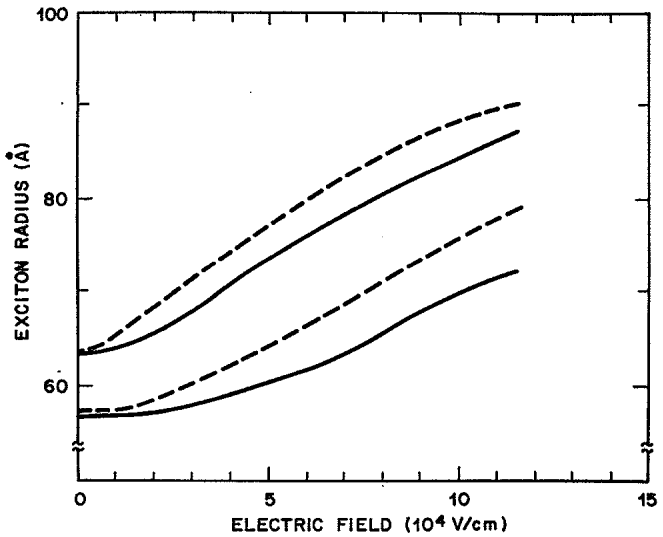

FIG. 14. Exciton radius as a function of electric field perpendicular to 95-Å GaAs quantum wells with $Al_{0.32}Ga_{0.68}As$ barriers for heavy-hole excitons and light-hole excitons as deduced from variational calculations. Solid lines, 57:43 split. Dashed lines, 85:15 split. Upper curves, heavy-hole exciton. Lower curves, light-hole exciton.

The integral over θ in Eq. (D1) is trivial and the integral over r can be performed, yielding

$$G(\gamma)\equiv\frac{2}{\lambda}\int_{r=0}^{\infty}\frac{r\exp(-2r/\lambda)dr}{\sqrt{\gamma^2+r^2}}$$
$$=\frac{2|\gamma|}{\lambda}\left\{\frac{\pi}{2}\left[\mathrm{H}_1\left[\frac{2|\gamma|}{\lambda}\right]-\mathrm{N}_1\left[\frac{2|\gamma|}{\lambda}\right]\right]-1\right\}, \tag{D2}$$

where $\mathrm{H}_1(u)$ is the first-order Struve function and N_1 is the first-order Neumann function or Bessel function of the second kind. The function $G(\gamma)$ limits to 1 as γ tends to zero although both H_1 and N_1 are singular for $\gamma=0$. H_1 was calculated directly by a power-series expansion, and N_1 was calculated using the zeroth- and first-order Bessel functions of the first kind and the zeroth-order Bessel function of the second kind[39] to give a look-up table for $G(\gamma)$. Using the look-up table for $G(\gamma)$ the final result for E_{PE} for given β_e, β_h, and λ was evaluated by numerical double integration over z_e and z_h.

Our procedure for calculating the binding energy E_B for a given field was first to deduce β_e and β_h for that field (from a separate variational calculation) then to evaluate E_{PE} (as discussed) and E_{KE}, adjusting λ variationally to minimize E_B. Our calculation differs from most others in that it attempts to account for the effect of finite-well depth by using effective-well widths; the comparison of our results and others (which are mostly infinite-well calculations) is good only if we use a mean well width for the other calculations which is approximately an average of our electron and hole effective-well widths.

The results of our calculations using the parameters given in Appendix C and a dielectric constant $\epsilon=12.15$ are summarized in Figs. 8(b) and 14. The exciton binding energies decrease in magnitude (this contribution is a positive energy shift overall) with applied field, with associated increases in the exciton radius $a\equiv\lambda/2$.

[1]W. Franz, Z. Naturforsch. **13a**, 484 (1958).
[2]L. V. Keldysh, Zh. Eksp. Teor. Fiz. **34**, 1138 (1958) [Sov. Phys.—JETP **7**, 788 (1958)].
[3]J. D. Dow and D. Redfield, Phys. Rev. B **1**, 3358 (1970).
[4]Q. H. F. Vrehen, J. Phys. Chem. Solids **29**, 129 (1968).
[5]R. Dingle, W. Wiegmann, and C. H. Henry, Phys. Rev. Lett. **33**, 827 (1974).
[6]D. A. B. Miller, D. S. Chemla, D. J. Eilenberger, P. W. Smith, A. C. Gossard, and W. Wiegmann, Appl. Phys. Lett. **42**, 925 (1983).
[7]T. Ishibashi, S. Tarucha, and H. Okamoto, in *Proceedings of the International Symposium on GaAs Related Compounds* [Inst. Phys. Conf. Ser. **63**, 587 (1981)].
[8]S. W. Kirchoefer, N. Holonyak, K. Hess, D. A. Gulino, H. G. Drickamer, J. J. Coleman, and P. D. Dapkus, Appl. Phys. Lett. **40**, 821 (1984).
[9]J. S. Weiner, D. S. Chemla, D. A. B. Miller, T. H. Wood, D. Sivco, and A. Y. Cho, Appl. Phys. Lett. **46**, 619 (1985).
[10]D. S. Chemla, D. A. B. Miller, P. W. Smith, A. C. Gossard, and W. Wiegmann, IEEE J. Quantum Electron. **QE-20**, 265 (1984).
[11]D. A. B. Miller, D. S. Chemla, D. J. Eilenberger, P. W. Smith, A. C. Gossard, and W. Wiegmann, Appl. Phys. Lett. **42**, 925 (1983).
[12]D. A. B. Miller, D. S. Chemla, P. W. Smith, A. C. Gossard, and W. Wiegmann, Opt. Lett. **8**, 477 (1983).
[13]Y. Silberberg, P. W. Smith, D. A. B. Miller, A. C. Gossard, and W. Wiegmann, Opt. Lett. **9**, 507 (1984).
[14]H. M. Gibbs, S. S. Tarng, J. L. Jewell, D. A. Weinberger, K. Tai, A. C. Gossard, S. L. McCall, A. Passner, and W. Wiegmann, Appl. Phys. Lett. **41**, 221 (1982).
[15]Y. Silberberg, P. W. Smith, D. A. B. Miller, B. Tell, A. C. Gossard, and W. Wiegmann, Appl. Phys. Lett. **46**, 701 (1985).
[16]T. H. Wood, C. A. Burrus, D. A. B. Miller, D. S. Chemla, T. C. Damen, A. C. Gossard, and W. Wiegmann, Appl. Phys. Lett. **44**, 16 (1984).
[17]T. H. Wood, C. A. Burrus, D. A. B. Miller, D. S. Chemla, T. C. Damen, A. C. Gossard, and W. Wiegman, IEEE J. Quantum Electron. QE-**21**, 117 (1985).
[18]D. A. B. Miller, D. S. Chemla, T. C. Damen, T. H. Wood, C. A. Burrus, A. C. Gossard, and W. Wiegmann, Opt. Lett. **9**, 567 (1984).
[19]D. A. B. Miller, D. S. Chemla, T. C. Damen, A. C. Gossard, W. Wiegmann, T. H. Wood, and C. A. Burrus, Appl. Phys. Lett. **45**, 13 (1984).
[20]D. A. B. Miller, D. S. Chemla, T. C. Damen, A. C. Gossard, W. Wiegmann, T. H. Wood, and C. A. Burrus, Phys. Rev. Lett. **53**, 2173 (1984).
[21]E. E. Mendez, G. Bastard, L. L. Chang, L. Esaki, H. Morkoc, and R. Fisher, Phys. Rev. B **26**, 7101 (1982).
[22]R. C. Miller and A. C. Gossard, Appl. Phys. Lett. **43**, 954 (1982).
[23]D. S. Chemla, T. C. Damen, D. A. B. Miller, A. C. Gossard, and W. Wiegmann, Appl. Phys. Lett. **42**, 864 (1983). In this paper we observed broadening and shift of the exciton peaks which we ascribed to fields parallel to the layers. However, with the improved sample geometries used in the present work, we now believe that these early results showed a combination of parallel and perpendicular fields together with some ohmic heating of the sample. In our present work, we have taken care to eliminate heating as a cause of any of the effects, and contacts have been improved to eliminate the formation of Schottky barriers which could give perpendicular fields in the parallel field sample.
[24]M. Yamanishi, T. Minami, and I. Suemune, in Extended Abstracts of the 15th Conference on Solid State Devices and Materials, Tokyo, 1983 (unpublished).
[25]M. Erman, P. Frijlink, J. B. Theeten, C. Alibert, and S. Gaillard, *Proceedings of the 11th International Symposium on GaAs and Related Compounds, Biarritz, 1984,* edited by J. A. Revill (Hilger, Bristol, U. K., in press).
[26]G. Bastard, E. E. Mendez, L. L. Chang, and L. Esaki, Phys. Rev. B **28**, 3241 (1983).
[27]J. A. Brum and G. Bastard, Phys. Rev. B **31**, 3893 (1985). This independent work provides a complementary but closely related calculation to that reported by ourselves briefly in Ref. 20 and in greater detail in the present paper for the perpendicular field electroabsorption. The wave functions used are slightly different, but excitonic effects are included in a manner similar to our own calculations. We have also carried out more direct calculations of the tunneling time of carriers out of the wells and obtained good absolute agreement of theory and experiment for the shifts, and in the present paper we have also repeated the calculations for the 57:43 split of the band discontinuities which has recently been favored.
[28]M. Yamanishi and I. Suemune, Jpn. J. Appl. Phys. **22**, L22 (1983).
[29]J. J. LePore, J. Appl. Phys. **51**, 6441 (1980).
[30]W. H. Knox, R. L. Fork, M. C. Downer, D. A. B. Miller, D. S. Chemla, C. V. Shank, A. C. Gossard, and W. Wiegmann, in *Ultrafast Phenomena IV,* edited by D. H. Auston and K. B. Eisenthal (Springer, New York, 1984), pp. 162—165; Phys. Rev. Lett. **54**, 1306 (1985).
[31]A. C. Gossard, W. Brown, C. L. Allyn, and W. Wiegmann, J. Vac. Sci. Technol. **20**, 694 (1982).
[32]J. C. Maan, G. Belle, A. Fasolino, M. Altarelli, and K. Ploog, Phys. Rev. B **30**, 2253 (1984).
[33]Y.-C. Chang and J. L. Schulman, Phys. Rev. B **31**, 2069 (1985).
[34]F. L. Lederman and J. D. Dow, Phys. Rev. **13**, 1633 (1976).
[35]M. Shinada and S. Sugano, J. Phys. Soc. Jpn. **21**, 1936 (1966).
[36]R. C. Miller, D. A. Kleinman, W. T. Tsang, and A. C. Gossard, Phys. Rev. B **24**, 1134 (1981).
[37]J. D. Dow and D. Redfield, Phys. Rev. B **5**, 594 (1972).
[38]C. Weisbuch, R. Dingle, and A. C. Gossard, Solid State Commun. **37**, 219 (1981).
[39]J. Hegarty, M. D. Sturge, C. Weisbuch, A. C. Gossard, and W. Wiegmann, Phys. Rev. Lett. **49**, 930 (1982).
[40]J. Singh, K. K. Bajaj, and S. Chaudhuri, Appl. Phys. Lett. **44**, 805 (1984).
[41]R. Dingle, in *Festkorperprobleme (Advances in Solid State Physics),* edited by H. J. Queisser (Pergamon, Braunschweig, 1975), Vol. XV, p. 21.
[42]R. C. Miller, D. A. Kleinman, and A. C. Gossard, Phys. Rev. B **29**, 7085 (1984).
[43]W. I. Wang, E. E. Mendez, and F. Stern, Appl. Phys. Lett. **45**, 639 (1984).
[44]D. Arnold, A. Ketterson, T. Henderson, J. Klem, and H. Morkoc, Appl. Phys. Lett. **45**, 1237 (1984).
[45]P. Dawson, G. Duggan, H. I. Ralph, K. Woodbridge, and G. W. Hooft, Superlattices, Microstruct. **1**, 231 (1985).
[46]T. W. Hickmott, P. M. Solomon, R. Fischer, and H. Morkoc (unpublished).
[47]Y. E. Lozovik and V. N. Nishanov, Fiz. Tverd. Tela (Leningrad) **18**, 3267 (1976) [Sov. Phys.—Solid State **18**, 1905 (1976)].
[48]G. Bastard, E. E. Mendez, L. L. Chang, and L. Esaki, Phys. Rev. B **26**, 1974 (1982).

[49]R. L. Greene and K. K. Bajaj, Solid State Commun. **45**, 831 (1983).
[50]Y. C. Lee and D. I. Lin, Phys. Rev. B **19**, 1982 (1979).
[51]N. N. Kolychev, B. B. Tarasov, A. M. Yaremko, and V. I. Sheks, Phys. Status Solidi B **98**, 527 (1980).
[52]T. F. Jiang, Solid State Commun. **50**, 589 (1984).
[53]There are some semantic problems and physical paradoxes associated with the use of the term "exciton binding energy" in this context which deserve some comment. First, the principal semantic problem is that there are no bound states of a system in a uniform electric field because the system can always tunnel to lower energy states and with the charged particles nearer to the "electrodes." However, it is reasonable to talk of an exciton as being a particle if it lives long enough to produce a recognizable resonance, which "orbits" before the exciton is destroyed; this is already the working definition even without field, because the exciton is not stable in the presence of phonons, and at room temperature in the quantum well the resonance is only just resolvable due to the phonon broadening. The use of the approximate separable wave function [Eq. (3)] also makes the problem of the definition of exciton binding energy deceptively simple, as the energy of the system as a whole then separates into the sum of three energies, E_e, E_h, and E_B. However, this is an artifact of the approximation; it encourages us to think that we can always conceive of the total shift of the exciton resonance as being the shift of the band gap (E_e+E_h) plus the change of exciton binding energy. In reality, the shift of the band gap and the shift of the exciton peak position are separate problems; it just happens that with this separable wave function the solution of the exciton problem involves the solution of the band-gap problem. Furthermore, the high-lying exciton states are probably not bound in any sense in the presence of the fields used here; hence, if we use the definition of binding energy as being the separation of the lowest bound state and the first unbound state, the first unbound state would not be the original lowest continuum state and E_B as used here would not be the binding energy. We refer to E_B as the exciton binding energy here for brevity and because it has a simple correspondence with the zero-field case. One physical paradox which arises from the separation of the problem is that the binding energy E_B actually reduces with field, tending to shift the exciton energy upwards. This is paradoxical because for a physical system of this symmetry the first consequence should be a reduction of energy. (If the exciton wave function were to remain totally unchanged in the presence of the uniform perpendicular field, its energy would not change because of its mirror symmetry; hence, given that the physical system always seeks the lowest energy state, the energy of the system cannot increase.) The resolution of this paradox is that the energy of the exciton as a whole does decrease; there is no requirement that an arbitrary contribution to that energy should decrease. Because of the arbitrariness of the binding energy, it is important to emphasize that the (Stark) shifts, which we discuss, are the total shifts of the exciton peaks, not the shifts in binding energy; there is, thus, no physical problem in having Stark shifts larger than the zero-field binding energy.
[54]R. Dingle and W. Wiegmann, J. Appl. Phys. **46**, 4312 (1975).
[55]D. D. Sell, J. C. Casey, and K. W. Wecht, J. Appl. Phys. **45**, 2650 (1974).
[56]B. Zaslow and M. E. Zandler, Am. J. Phys. **35**, 1118 (1967).
[57]J. W. K. Hang and A. Kozucki, Am. J. Phys. **47**, 1005 (1979).
[58]G. Q. Jassoun, Am. J. Phys. **49**, 143 (1983).
[59]H. A. Bethe and E. E. Salpeter, *Quantum Mechanics of One and Two Electron Atoms* (Springer, Berlin, 1957).
[60]L. O. Landau and E. M. Lifshitz, *Quantum Mechanics—Nonrelativistic Theory* (Pergamon, New York, 1981), Chaps. VII and X.
[61]A. Rabinowitch and J. Zak, Phys. Rev. B **4**, 2358 (1971).
[62]T. Lukes and G. A. Ringwood, Physica **84A**, 421 (1976).
[63]F. M. Fernandez and E. A. Castro, Physica **111A**, 334 (1982).
[64]M. Abramowitz and I. A. Stegun, *Handbook of Mathematical Functions* (National Bureau of Standards, Washington, D.C., 1964).
[65]The computer solution for the particle transmission of quantum-well structures was developed and provided by G. A. Baraff.